Journal of Membrane Science 643 (2022) 119997

Contents lists available at ScienceDirect

Journal of Membrane Science

journal homepage: www.elsevier.com/locate/memsci

Enhancing long-term accuracy and durability of wastewater monitoring using electrosprayed ultra-thin solid-state ion selective membrane sensors

Yingzheng Fan [a], Xin Qian [b], Xingyu Wang [a], Thomas Funk [a], Brianna Herman [a], Jeffrey R. McCutcheon [b], Baikun Li [a,*]

[a] Department of Civil & Environmental Engineering, University of Connecticut, Storrs, Connecticut, 06269, USA
[b] Department of Chemical and Biomolecular Engineering, University of Connecticut, Storrs, Connecticut, 06269, USA

ARTICLE INFO

Keywords:
Electrospray
Solid-state ion selective membrane sensor
Controllable membrane thickness
Ion diffusion and response model
Reading (mV) drifting
Continuous and long-term wastewater monitoring

ABSTRACT

Current membrane deposition approaches (e.g., drop-casting, spin-coating) for solid-state ion selective membrane (S-ISM) sensors suffer from problems including sensor material waste, uncontrollable membrane thickness (100–200 μm), loose contact between sensing membrane and electrode surface, long response time (e.g., >20 s) and poor reading stability (e.g., >3 mV/h). This study addressed these challenges by depositing ISM through electrospray printing technology and enabling accurate and continuous monitoring in water and wastewater. Specifically, the final droplet size and the splash diameter of the electrosprayed droplets deposited a particularly tunable, high resolution and ultra-thin (thickness: ~1 μm) membrane on the electrode surface, which immensely shortened the sensor response time (9.2 s), strengthened the adhesion between the ISM and the electrode surface, mitigated the formation of water layer in the S-ISM sensor entity, and ultimately enhanced the sensor reading stability (reading drifting <0.66 mV/h). Additionally, the ion diffusion model developed in this study confirmed that fast ion diffusion in the electrosprayed S-ISM polymer matrix effectively shortened the response time of sensors. Electrosprayed S-ISM sensors without anti-fouling protection exhibited high stability and accuracy with an error of less than 2.9 mg/L after continuously monitoring wastewater for 10 days, revealing a great potential for further enhancement.

1. Introduction

Solid-state ion-selective membrane (S-ISM) sensors have gained enormous attention for water quality monitoring in the past decade [1,2]. Distinct features such as high selectivity for water contaminants (e.g., ammonium, nitrate, lead, potassium), small sensor size (e.g., diameter at mm and cm magnitude), simple instrumentation and easy deployment make this modest design of potentiometric sensors advantageous over other analytical techniques (e.g., biomimetic, colorimetric, voltammetric and conductometric sensors) [3,4]. However, the commonly approach for depositing S-ISM onto the substratum electrode surface (e.g., graphite) is manual drop-cast using a solution of diluted cocktail containing ionophore and polymer matrix [5–7], which poses several problems such as sensor material waste, uncontrollable membrane thickness (100–200 μm), loose contact between sensing membrane and electrode surface, and resulting in long response time (e.g., >20 s) and poor stability (e.g., >3 mV/h) [8,9]. Therefore, a less-material-consuming, uniform, consistent and reproducible approach is urgently needed for depositing ultra-thin (thickness: <5 μm) S-ISM in order to advance the sensor performance, especially for accurate monitoring in water and wastewater.

Several new deposition approaches have been attempted to enhance the coating quality of S-ISM. Spin-coating was applied to uniformly deposit the K^+ selective cocktails onto the electrode (e.g., glassy carbon) [10], but the spinning step swept away most cocktail after deposition, resulting in material waste. Dip coating was developed by dipping one end of the conductive thread in the ion-selective cocktail to form membrane [11], but the membrane thickness suffered from poor reproductivity ($R^2 < 0.9$). In contrast, electrospray approaches that utilize the Coulombic dispersion of droplets can achieve an ultra-thin, reproducible, and uniform membrane [12]. Compared with spin-coating and dipping, the additive electrospray technique can produce thin films with exceptional control of membrane thickness [13]. Electrospray has been used for mass spectrometry analysis [14],

* Corresponding author.
E-mail address: baikun.li@uconn.edu (B. Li).

https://doi.org/10.1016/j.memsci.2021.119997
Received 28 August 2021; Received in revised form 6 October 2021; Accepted 18 October 2021
Available online 23 October 2021
0376-7388/Published by Elsevier B.V.

deposition of organic thin film and biomolecules (e.g., photosynthetic organisms, proteins and DNA) onto Light-emitting diode (LED) devices [15] and conducting oxide glass slide [16], deposition of nanoparticles onto gas sensors (e.g., Co_3O_4 nanoparticles acetone gas sensor [17], nanostructure graphene oxide gas sensor [18]), and in various membrane fabrication and modification. Especially, the use in membrane applications strongly unveils the capability of electrospray to create ultra-thin films (even those far less than 1 μm in thickness) that are defect free. Such a benefit could have value in the preparation of S-ISM sensors which, up until now, has never deployed electrospray in fabrication.

The breakthroughs of this study lay in advancing the membrane characteristics of S-ISMs through electrospray printing technology and systematically determining the impacts of membrane properties on the

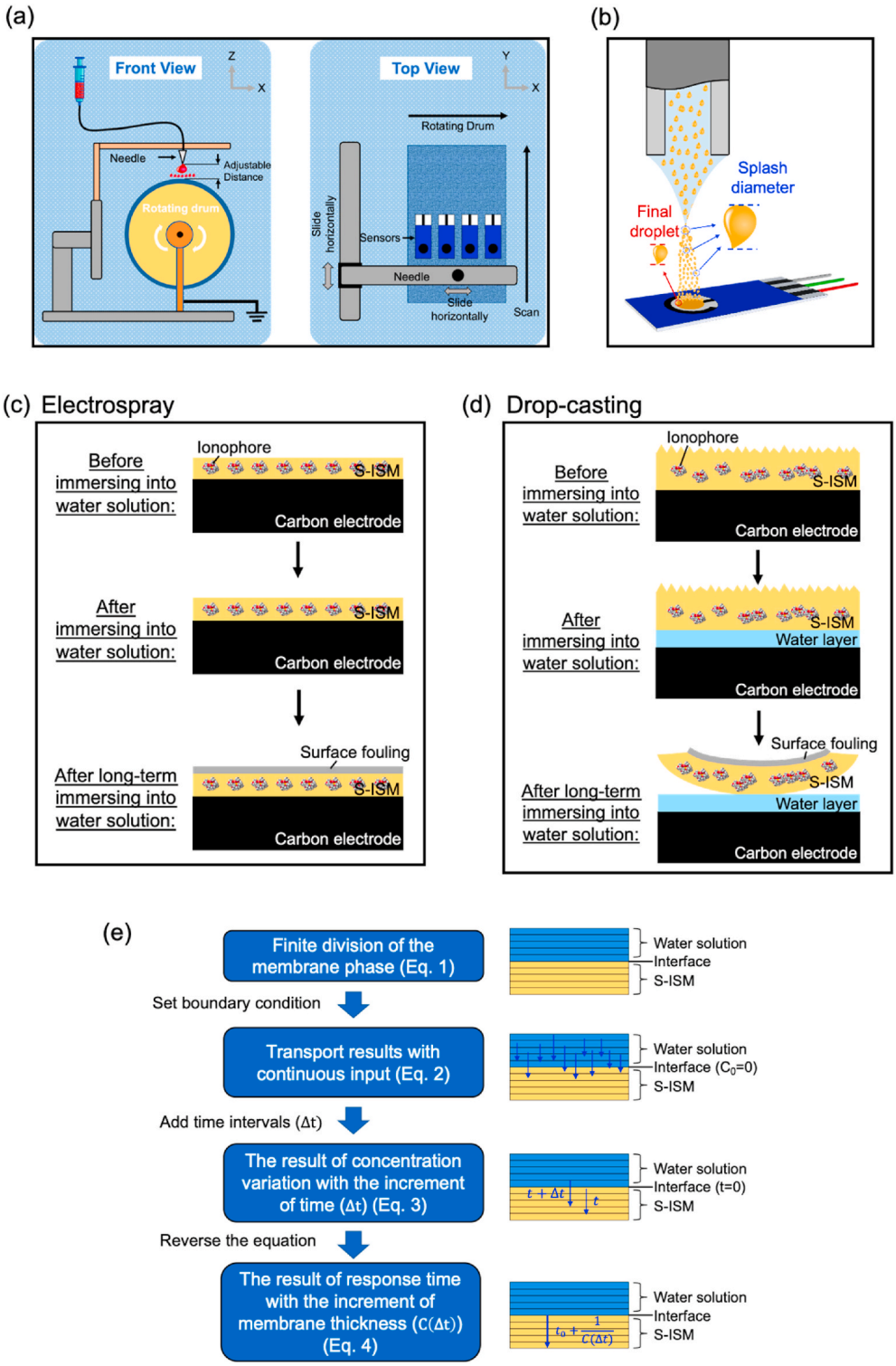

Fig. 1. (a). The fabrication process of electrospray S-ISM. (b). The final droplet size and the splash diameter of the electrosprayed droplets. Mitigated water layer formation and enhanced ionophore distribution in the (c) electrosprayed S-ISM sensor compared with the regular (d) drop-casting S-ISM sensor. (e). Streamline diagram of the ion diffusion and membrane response model.

sensor performance in water and wastewater monitoring. Specifically, different layers of the diluted ISM cocktails were electrosprayed onto the carbon electrode surface to achieve a thin membrane for enhanced member morphology and sensor performance. Due to the small droplet size (Fig. 1a), the S-ISM thickness was expected to be thin and controllable in thickness by the tens of nanometers. By lessening the cocktail concentration and reducing the membrane thickness, the material cost of S-ISM sensors is expected to be less than $1 persensor. Furthermore, an innovative ion diffusion model in the phase of membrane was developed in this study to elucidate the correlation between the sensor response time and the S-ISM membrane thickness, which can be carefully controlled using this method. Understanding gained from this model could immensely facilitate the determination of optimal thickness of the thin membrane and accelerate membrane fabrication using electrospray technology. Additionally, since most solvent evaporated during its travel toward the sensor surface, electrosprayed layers could achieve better surface affinity with the electrode surface than the drop cast cocktail [19]. Therefore, the electrosprayed ISM was expected to strengthen the membrane adhesion with the carbon electrode [20], mitigate the formation of water layer between the sensing membrane and electrode, and thus alleviating the sensor reading (mV) drift and enhancing data accuracy of monitoring in real-world water and wastewater.

Built upon the ammonium (NH_4^+) S-ISM sensor platform that we have developed for wastewater monitoring [1], five tasks were carried out in this study. First, the ultra-thin S-ISM (thickness: 1 μm) was fabricated using the electrospray printing technology, and the membrane thickness was determined through the cross-section of SEM observation. Second, the sensitivity and accuracy of the ultra-thin electrosprayed S-ISM sensors were examined and compared with the regular drop-casting sensors. Third, the ion diffusion model in the phase of membrane was established to relate membrane thickness with the sensor response time to different concentrations. Fourth, the mechanisms of the electrosprayed membrane to reduce water layer formation were explored using adhesion tests and water layer tests. Fifth, the practical accuracy and mechanical stability of the ultra-thin electrosprayed S-ISM sensors were examined continuously in real-world wastewater for 14 days, during which the S-ISM sensor morphology was characterized and correlated with the sensor performance.

2. Materials and methods

2.1. Fabrication of S-ISM NH_4^+ sensors using drop-casting and electrospray methods

The sensor substrate (length: 3.5 cm, width: 1.5 cm, thickness: 0.1 cm) was fabricated using screen-printing (eDAQ, ET083). The 200 mg NH_4^+ ISM cocktail was prepared by dissolving ammonium ionophore I (6.9% weight by weight, w/w; nonactin, Sigma-Aldrich), plasticizer 2-nitrophenyloctylether (NPOE, 59.6% w/w, Sigma-Aldrich), and potassium tetrakis(4-chlorophenyl)- borate (0.7% w/w, Sigma-Aldrich, served as cation exchanger), and poly(vinyl chloride) (PVC, 32.8% w/w, high molecular weight, Sigma-Aldrich, served as the polymer matrix) in 5000 μL of tetrahydrofuran (THF, ≥99.5%, Sigma-Aldrich) and then mixed ultrasonically for 60 min. In the drop-casting approach previously reported [1], 15 μL NH_4^+ ISM cocktail was carefully drop-casted onto the surface of the carbon-based working electrode (radius: 2.5 mm) using a single channel pipette, and then dried at room temperature over 48 h under N_2 and a lightless environment to form drop-casting S-ISMs. Here, the mechanism of S-ISM ammonium sensors relied on the selective affinity of the ionophore for targeted NH_4^+ ions [1]. This affinity drives the diffusion of NH_4^+ ions into the S-ISM membrane, causing the potential (mV) change in the charge state of the electrodes. This potential change followed the rule of electrochemical Nernstian slope ($\Delta E = \frac{2.3026RT}{zF}$), which is closely related with the absolute temperature, Faraday constant, gas constant, and the valency of the targeted ions, but is not corresponded with the density of ionophore in the S-ISM sensor [21,22].

In the electrospray process, the sensor substrate was attached to the drum rotating at 14 rpm, and then the cocktail in the syringes was sprayed at a fixed flow rate of 3.9 mL/h onto the carbon-based electrode (Fig. 1a). The cocktail was extruded out of the needle tip, which was mounted on the plastic holder with a tip-to-drum distance of 4.5 cm [19]. The positive voltage applied on the needle tip was set at 6.6 kV provided by a high-voltage power source [19]. These parameters were maintained for electrospraying different batches of cocktails since the spray parameters always depended on the solvent properties at the low solute concentration. Consequently, by forming the spray pattern in cone and jet mode, the spray comprising the finest droplets was deposited onto the sensor surface as a circular deposition area, which finally integrated into a thickness-controllable thin layer (Fig. 1b). The stage carrying two needles was mounted on a code-driven screw slide to move back and forth along the drum axial direction. The needles were rastered along the length of the drum by a Velmex controller at a speed of 350 μm/s for 16 cm and then returned to the original position if more than one layer was required [13]. The electrospray process was conducted at 23 °C and 16% relative humidity to maintain uniform solution viscosity [23]. After the S-ISM membrane was electrosprayed onto the carbon electrode, the sensor was dried at room temperature over 48 h under N_2 and a lightless environment to form the S-ISM. Different thicknesses of S-ISM were attained by adjusting electrospray layers (5, 15, 25, 35, 45, 55, 65, and 75 layers). A minimum of 5 layers were required to form an integrated layer of S-ISM and fully cover the carbon electrode surface. Thereby, the thinnest S-ISM was 5-layer membrane, and an interval of 5 layers was used to fabricate the electrospray layers with different thicknesses (e.g., 5, 15, 25, 35, 45, 55, 65, and 75 layers).

2.2. Thickness measurement of the S-ISM sensors

The S-ISMs fabricated with electrospray and drop-cast were individually cut into circle-based membrane samples (radius: 2.5 mm) using a scissor. These samples were then submerged into the liquid nitrogen for approximately 30–60 s and immediately taken out to be fractured to expose a clean edge for imaging. Subsequently, these semicircle-shaped samples were adhered onto copper conducting tapes and fixed on the sample stages to allow the cross-sectional observation. These S-ISM samples were characterized using a scanning electron microscope (SEM, FEI Nova NanoSEM 450) at an accelerating voltage of 10.0 kV, after sputter-coating with gold-palladium layer (Polaron E5100 Sputter Coater) for 2 min. The average thickness of S-ISM was determined using the FIJI (ImageJ) software.

2.3. Characterization of the S-ISM sensors

For sensor calibration, the S-ISM sensors fabricated with electrospray and drop-casting methods were individually submerged into the 1 mg/L NH_4Cl water solution (100 mL). The solution was continuously stirred at 100 rpm via Thermolyne Cimarec-top stirring plate. Subsequently, the NH_4 concentration was sequentially increased from 1 mg/L to 2, 4, 8, 16, 32–64 mg/L by adding 100 g/L concentrated NH_4Cl solution. The reading (mV) of the NH_4^+ S-ISM sensor was recorded at the interval of 0.1 s using a multichannel electrochemical workstation (CHI 660D potentiostat).

A water layer test was the standard method towards S-ISM sensors to verify the water layer formation between the S-ISM and electrode surface [24], and thus it has been used as the indicator to assess the S-ISM sensor stability by alternately immersing into primary and interfering ion water solution (Fig. 1c and d) [25]. Specifically, the S-ISM sensors fabricated using electrospray and drop-casting were simultaneously immersed into the primary ion solution (NH_4Cl, 0.1 M) for ~7200 s to obtain an equilibrium with the solution. Subsequently, both sensors

were switched into the interfering ion solution (NaCl, 0.1 M) for ~7200 s to ensure interfering ions to transport through the membrane and achieve a new equilibrium. Finally, these two sensors were taken back to the primary ion solution (NH_4Cl, 0.1 M) and submerged for another ~7200 s to equilibrate with the solution. The entire process of water layer test was continuously recorded using a multichannel electrochemical workstation (CHI 660D potentiostat) to obtain the potential readings (mV) of both sensors at the interval of 10 s.

The adhesion test of S-ISM NH_4^+ sensors was performed using a transparent tape (Gorilla Tape) to tear up the S-ISM membrane from the carbon-based working electrode of the sensor, as previously reported [25]. Both electrospray and drop-casting sensors were immersed into the water solution for 7 days before the adhesion test. Specifically, a Gorilla™ tape was first stuck onto the S-ISM membrane surface for 30 s and then rapidly pulled off from the membrane. The membrane would be teared up onto the tape if the adhesion between the membrane and the electrode is weak, while the membrane would stay on the electrode if this adhesion between the membrane and the electrode is strong.

Electrochemical impedance spectroscopy (EIS) was performed to compare the resistance of the S-ISM fabricated with electrospray and drop-casting. The EIS measurement was conducted in 0.1 M KCl solution. The results were recorded in the frequency range from 100 kHz to 0.1 Hz using an excitation amplitude (ΔE_{ac}) of 10 mV. Additionally, these data were fitted based on the equivalent circuit models in the ZSimpWin software.

2.4. The model of response time and membrane thickness

To determine the response time under the changes of concentration, the S-ISM sensors fabricated using the electrospray and drop-casting methods were simultaneously submerged into the 1 mg/L NH_4Cl water solution (100 mL) for 30 s. The solution was continuously stirred at 100 rpm via Thermolyne Cimarec-top stirring plate. Subsequently, 60 μL of 100 g/L concentrated NH_4Cl solution was added into the NH_4Cl water solution. The reading (mV) of the NH_4^+ S-ISM sensors was recorded at the interval of 0.1 s using a multichannel electrochemical workstation (CHI 660D potentiostat). The response time was defined as the time required for the sensor readings (mV) to change from its initial steady state to the final steady value.

In order to elucidate the relationship between the S-ISM sensor's response time and membrane thickness, a sensor response model was developed based on the ion diffusion process in the phases of the membrane (Fig. 1e) [26]. This model included the finite division of the membrane phase for calculating the concentration of the main ion in each divided layer of the membrane, which was described as Eq. (1):

$$C(t+\Delta t) = C_j(t) + \left\{C_{j-1}(t) - C_j(t)\right\}\frac{dt}{d^2z}\cdot D - \left\{C_j(t) - C_{j+1}(t)\right\}\frac{dt}{d^2z}\cdot D \quad (1)$$

Where d_z is the thickness of the elementary layers in the membrane, D is the diffusion coefficient, $C_j(t)$ is the concentration of the main ion at the instant of time t in layers j of the sensing membrane, Δt is the time increment used in equations, so, $V(t+\Delta t)$ is the diffusion velocity of the main ion at the next instant of time $t+\Delta t$. The boundary condition was set equal to the solution concentration ($C_{solution}$) at membrane surface and the concentration ($C_0 = 0$) at the interface between the membrane and electrode at the initial state ($t = 0$). Therefore, based on continuous input of the membrane diffusion process, the equation can be calculated to Eq. (2):

$$C(z,t) = \frac{C_{solution}}{2}\cdot \mathrm{erfc}\left(\frac{z}{2\sqrt{Dt}}\right) \quad (2)$$

Based on the relationship between the concentration, membrane layers and time, the concentration variation with the increment of time can be described as Eq. (3):

$$C(\Delta t) = C(z,t) = \frac{C_{solution}}{2}\cdot \mathrm{erfc}\left(\frac{(z+\Delta z)}{2\sqrt{D(t+\Delta t)}}\right) - \frac{C_{solution}}{2}\cdot \mathrm{erfc}\left(\frac{z}{2\sqrt{Dt}}\right) \quad (3)$$

According to the concentration variation rate and base response time (t_0) for electrospray S-ISM, we could subsequently obtain the relation between the response time and membrane thickness in Eq. (4):

$$R_t = t_0 + \frac{1}{C(\Delta t)} = t_0 + \frac{1}{\frac{C_{solution}}{2}\cdot \mathrm{erfc}\left(\frac{(z+\Delta z)}{2\sqrt{D(t+\Delta t)}}\right) - \frac{C_{solution}}{2}\cdot \mathrm{erfc}\left(\frac{z}{2\sqrt{Dt}}\right)} \quad (4)$$

According to Eq. (4), the membrane response model was plotted using the python code (Text S1) to explore the response acceleration of the thin membrane fabricated by electrospray technology.

2.5. Continuous tests of the S-ISM NH_4^+ sensors in real-world wastewater

The accuracy and mechanical stability of the electrosprayed and drop-cast S-ISM NH_4^+ sensors were examined by immersing both sensors into the parafilm sealed beakers containing real-world wastewater taken from the effluent of the UConn wastewater treatment plant (Table S1) and continuously monitoring for 14 days. The potential readings (mV) of both sensors were individually recorded every 30 s using an electrochemical workstation (CHI 660D). Subsequently, all potential readings (mV) were converted to ammonium (NH_4^+) concentration (mg/L) using the calibration results over 14 days. All the measurements were triplicated, and the average values were calculated. The accuracy of the sensor was validated by measuring the NH_4^+ concentration of the wastewater in the beaker using the dimethylphenol method (TNT 835/836) with a Hach DR2800 once per two days throughout the 14-day period. The sensor surface morphology was observed using a SEM before and after the 14-day test in wastewater, following the protocols described previously [25].

3. Results and discussion

3.1. Thickness determination of electrosprayed S-ISM sensors

The cross-sectional SEM images of the S-ISM membranes fabricated using different electrospray layers (5, 15, 25, 35 and 45 layers) (Fig. 2a) illustrated that the membrane thickness increased with the number of electrospray layers, with the thickness of the S-ISMs from 5, 15, 25, 35 and 45 layers as 1.05 ± 0.14 μm, 3.03 ± 0.17 μm, 5.07 ± 0.44 μm, 6.78 ± 0.90 and 9.16 ± 0.51 μm, respectively. Interestingly, an excellent linear relation ($R^2 = 0.9983$) was attained with a slope of 0.1987 between the membrane thickness and the number of layers (Fig. 2b), indicating a mean thickness of 198 nm was achieved per layer. Control of thickness per layer was evidently consistent and reproducible in electrospray. This exceptional thickness control was determined by the final droplet size and the splash diameter of the electrosprayed droplets (Fig. 1b). Specifically, the final droplet size was the size of the aerosol drops when it arrived at the substrate surface and the splash diameter was defined as the size of the droplet pattern after it hit the substrate. Based on the Gañán-Calvo model [27], these two parameters could be minimized by reducing the flow rate of the solution, expanding the tip-to-drum distance and raising the applied voltage potential. Lower flow rate could result in smaller droplet size during its travel, and increasing the tip-to-drum distance and voltage meant more evaporation of solvent as it travelled through the air. We adjusted the tip-to-drum distance, the flow rate of the extruded solution and the voltage applied on the nozzle tip in order to maximize the spray angle (Fig. 1a). This guaranteed a homogeneous and stable deposition of the polymer on the substrate (the carbon electrode in this study), which was reflected as reproducibility and consistency of membrane thickness via this electrospray technique.

More importantly, through electrospray technique, the S-ISM

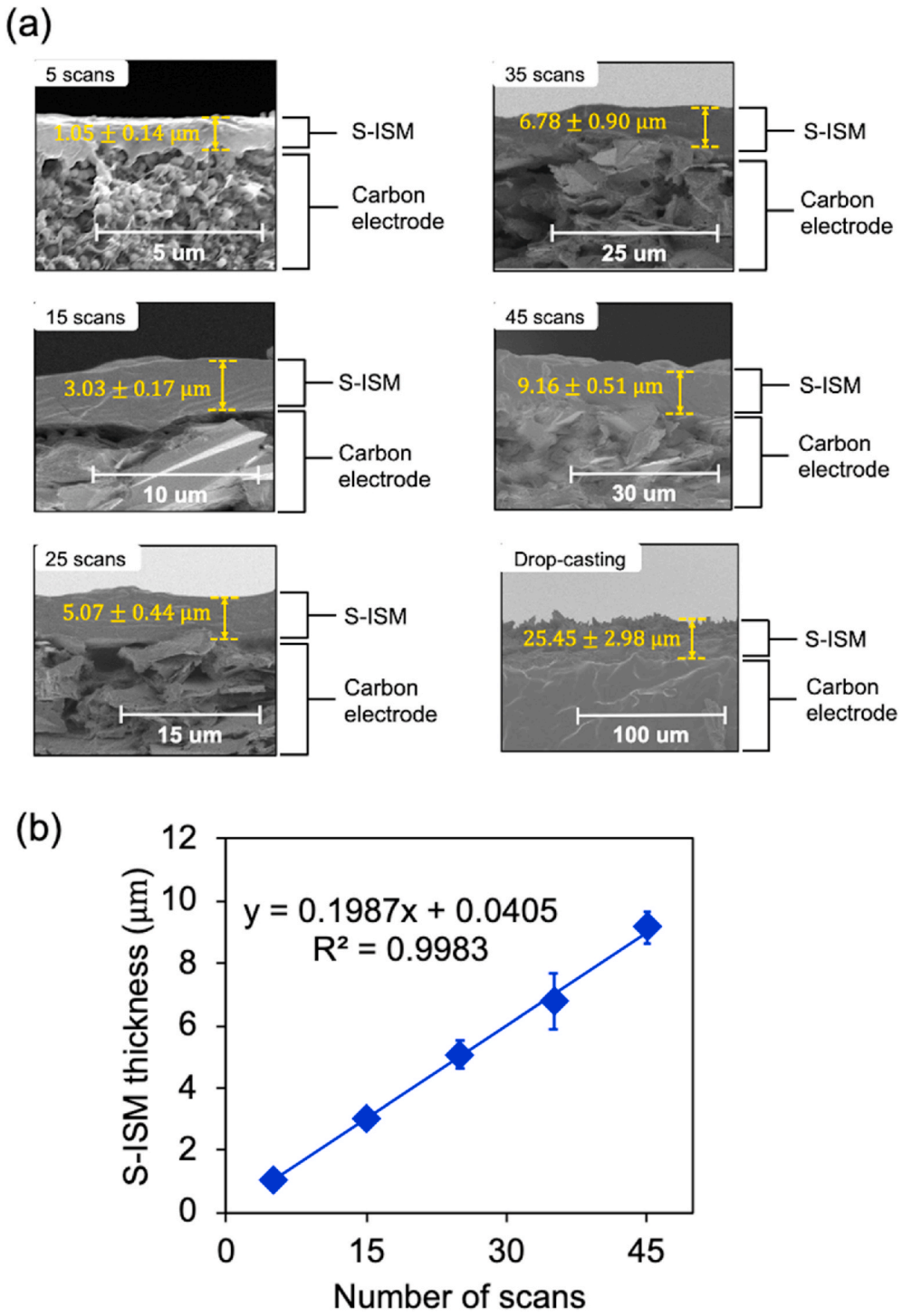

Fig. 2. (a). The cross-sectional SEM images of S-ISM membranes fabricated from different electrospray layers (5, 15, 25, 35 and 45 layers) and drop-casting. (b). The relationship between S-ISM thickness (μm) and number of electrospray layers.

thickness can be reduced to as little as 1.05 ± 0.14 μm (~1 μm), which was far thinner than the S-ISM sensors reported. Most traditional drop-casting S-ISM was around 200 μm [28], such as a lead (Pb^{2+}) selective membrane with the thickness of ~235 μm based on Diazadibenzo-18-crown-6 ionophores [29] and ~90 μm thick potassium (K^{+}) ion selective membrane over poly(3,4-ethylenedioxythiophene) (PEDOT) solid contact [30]. A series of ion selective membrane with the thickness of ~50 μm was developed in the microfluidic chip [31]. The thinnest S-ISM achieved using drop casting in our previous study was 25.45 ± 2.98 μm (Fig. 2a) [32]. Therefore, the ~1 μm membrane thickness obtained using electrospray was expected to greatly reduce lag time for sensor response.

3.2. Sensitivity, accuracy and stability improvements of the electrosprayed S-ISM sensors

Sensitivity is a critical index to evaluate the sensor performance in water and wastewater [33]. As a potentiometric device, S-ISM sensors have a limitation of sensitivity due to the Nernst logarithmic dependence ($\Delta E = \frac{2.3026 \times RT}{zF} \log(c)$) between potential (mV) and concentration

(mg/L) [34]. For example, 1 mV potential difference means a ~4% variation in ion concentration for the monovalent ion (e.g., NH_4^+, NO_3^-) [34]. Thereby, high sensitivity is particularly crucial for S-ISM sensors in water and wastewater monitoring where the concentration interval is relative narrow (e.g., <0.5 mg/L). Here, S-ISM sensors were examined in ammonium solutions ranging from 1 to 64 mg/L, i.e., spanning typical ammonium concentration for municipal wastewater [35]. According to the Nernst equation conversion, this ultra-thin electrosprayed S-ISM sensor (~1 μm) not only exhibited the high Nernstian slope of 55.28 mV/dec, but also possessed the excellent linear response (R^2: 0.9998) (Fig. 3a). This performance considerably exceeded the S-ISM sensors previous reported, such as polyaniline and poly(*o*-phenylenediamine)-modified S-ISM sensor (54.99 mV/dec, $R^2 = 0.995$) [36], multi-walled carbon nanotubes (MWCNTs)-based S-ISM sensor (55.1 mV/dec, $R^2 = 0.997$) [37], and regular drop-casting S-ISM sensor (51.307 mV/dec, $R^2 = 0.9997$, Fig. 3b). For potentiometric selective membrane sensors, the measured potential (mV) was closely related to the surface chemisorption of the sensing membrane, without the need for extensive transmembrane material transport [24]. Thereby, the sensitivity (Nernst slopes) of S-ISM sensors highly depended on the distribution of S-ISM membrane materials (e.g., ionophore, Polyvinyl Chloride (PVC)). Here, the EDS image of electrosprayed S-ISM surface (Fig. 3c) clearly displayed the more evenly distributed elements (e.g., Chloride, the main component in PVC as the ionophore supporting matrix [24]) than the drop-casting counterpart (Fig. 3d), confirming the prominent performance of the electrosprayed sensors in water monitoring.

Furthermore, the S-ISM sensors can suffer from reading (mV) drift caused by water layer formation between the deposited S-ISM membrane and the carbon electrode (Fig. 1c) [38], which severely deteriorates the reading accuracy for long-term continuous monitoring. The water layer test was performed to assess such water layer formation after immersing alternately in NH_4Cl and NaCl solutions for 21,600 s. The drop-casting sensor exhibited a clear positive potential drift of ~42 mV, when the solution was changed from NH_4^+ to Na^+ and then a negative reading drifts (mV) also of ~19 mV when returning from Na^+ back to NH_4^+ (Fig. 4a). This immense reading drift (>3.3 mV/h) evidently proved the water layer formation between the drop-casting membrane and electrode surface. In this case, the ion-to-electron transducer was considered to fail partially [39]. As the water layer continued to spread cross the interface of the membrane and electrode, the adhesion between the membrane and electrode might be further destroyed, finally resulting in mechanical failure by delamination (Fig. 1c) [40,41]. On the other hand, the ultra-thin electrosprayed S-ISM sensor presented more stable potential variations of ~4 mV in the water layer tests when switching from the Na^+ solution to the NH_4^+ solution at the same time scale (21,600 s) (Fig. 4a). This stability (potential variation: 0.66 mV/h) was even comparable to previous water-repellent studies using a much more complex configuration of PEDOT (poly(3,4-ethylenedioxythiophene)) [30], graphdiyne oxide [42] or polymer/-carbon nanocomposites [43] as the solid contact. The minimization of water layer formation was mainly attributed to the enhancement of S-ISM adhesion to the carbon electrode (Fig. 1d), which was further validated by tearing the membrane from the electrode surface using a scotch tape (the inserted images, Fig. 4a). After being immersed in a water solution for 7 days, the drop-casting S-ISM membrane was wholly teared up by the tape, while the electrosprayed membrane was still firm on the electrode surface and nearly kept its intactness during the adhesion tape test. Because each electrospray printing layer only deposited a tiny amount of S-ISM polymer solute on the carbon electrode surface, the next layer deposited onto the previously printed layer carries certain amount of excessive evaporated solvent (e.g., tetrahydrofuran), which redissolves the previously printed layers and consequently enhances the affinity of the S-ISM to the electrode (Fig. 4b) [20]. Therefore, this ultra-thin electrosprayed S-ISM sensor effectively minimized the water layer formation and suppressed the membrane delamination, and thus successfully alleviating the reading (mV) drift and enhancing the sensor reading stability.

3.3. Response acceleration of electrosprayed S-ISM sensors

Response time indicates how quickly a monitoring system can

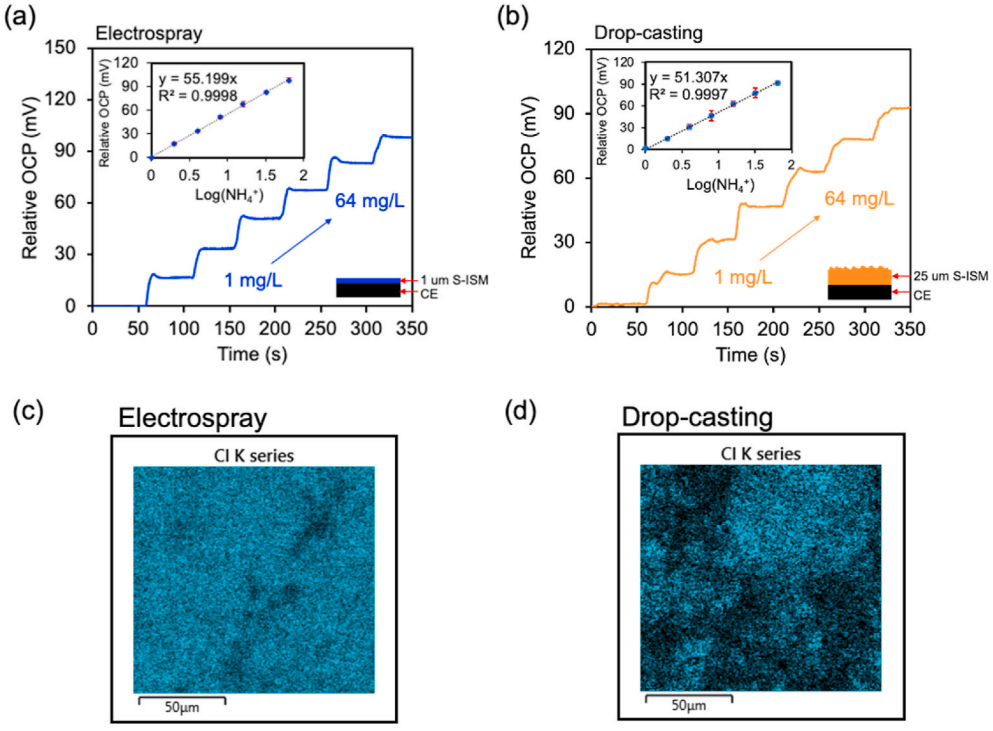

Fig. 3. Sensitivity and accuracy of ultra-thin electrosprayed S-ISM sensor (a) and regular drop-casting S-ISM sensor (b). EDS images of (c) electrosprayed and (d) drop-casting S-ISM surface (Selected element: chloride).

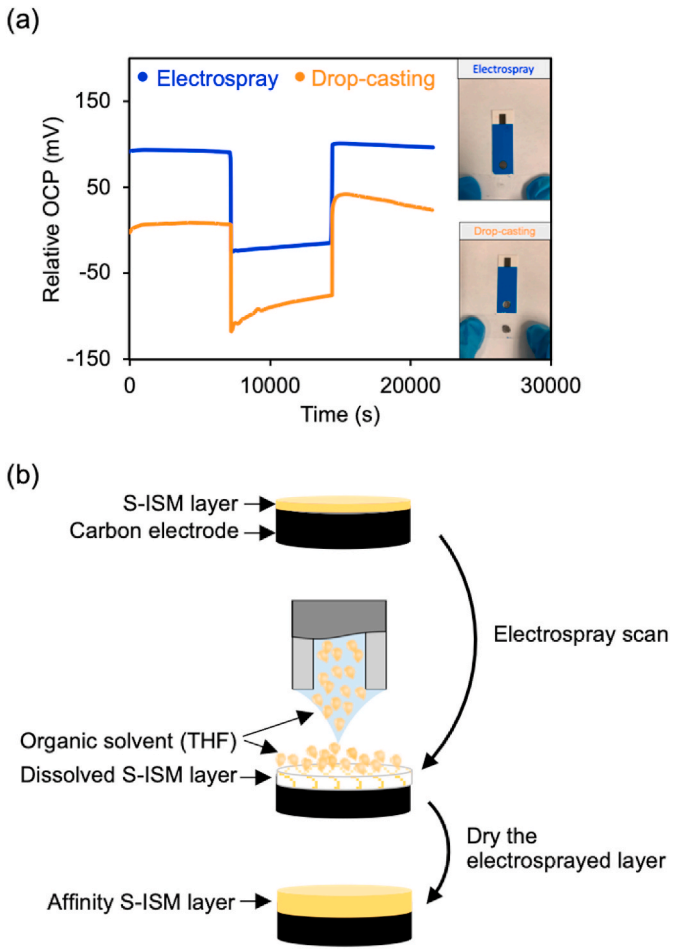

Fig. 4. (a). Water layer test of the electrosprayed and drop-casting S-ISM sensors. (The inset schematics was the adhesion test of ultra-thin electrosprayed and drop-casting S-ISM after being in water solution for 7 days. (b). Re-dissolution of the previously printed layer by organic solvent during electrospray and the consequently enhanced affinity of S-ISM to the carbon electrode surface.

respond to a change of the test solution. In this study, the ultra-thin electrospray S-ISM sensor noticeably exhibited a faster response (9.2 s) than the drop-casting sensor (22.5 s) after 60 μL NH_4Cl solution was introduced to the solution (Fig. 5a). In fact, this response time (9.2 s) was faster than other S-ISM sensors reported, including the modified BGO/AlFu MOF (boron doped graphene oxide-aluminum fumarate metal organic framework) nano-composite ion-selective electrode (~13 s) [44], noble metal nanostructured layered Li^+ ion selective electrode (~15 s) [45], and polyaniline-coated benzene sulfonate ion selective electrode (~20 s) [46]. Undoubtedly, this rapid response was attributed to the low thickness (1 μm) of S-ISM, which could be explained by the response model based on the diffusion process in the phases of the membrane (Eqs. (1)–(4)) [26]. In this model, the finite difference method was used to divide the membrane phase into a number of layers of finite thickness (Fig. 1e, Eq. (1)). The concentration profile between the next layers was considered as linear response due to its extremely small (0.005 mg/L) variations. This sufficient small concentration profile ensured the accuracy and precision of the model results. Therefore, the model simulation data (blue dots, Fig. 5b) almost covered all of the experimental data (black dots, Fig. 5b) with a high R^2 value ($R^2 > 0.85$), demonstrating an excellent fitting for the electroporated S-ISM sensors' response with different thicknesses (1–15 μm). Comparatively, previous sensor models (e.g., Controlled-Potential Membrane Response Model [47], Time-Dependent Diffusion Model for electrode response [48]) cannot divide the membrane phase till to such small (<0.01 mg/L) profiles, since the range of their fitting experimental results were broad (>100 μm) and difficult to sustain consistency, which resulted in the low R^2 value ($R^2 < 0.5$) towards the model fitting and was unable to truly characterize the relationship between the sensing membrane and the response time in such thin S-ISM thickness range (1–15 μm). Conversely, our model clearly illustrated that a shorter ion diffusion distance in the electroporated S-ISM phase (1–15 μm) could facilitate the ion diffusion process when the primary ion concentration varied in the water solution. Besides, the Nyquist plots of Electrochemical Impedance Spectroscopy (EIS) (Fig. 5a) exhibited the lower resistance (14.5 kΩ) of this ultra-thin electrospray S-ISM compared with drop-casting S-ISM resistance (37.6 kΩ), confirming the faster ion diffusion in the electrosprayed S-ISM polymer matrix and the shortened response time for water monitoring.

3.4. *Continuous monitoring of wastewater for 14 days using electrosprayed S-ISM sensors*

Continuous performance of the ultra-thin electrosprayed and drop-casting NH_4^+ S-ISM sensors was examined side-by-side for 14 days in real-world wastewater. The ultra-thin electrosprayed S-ISM sensors exhibited much smaller reading drifts (Fig. 6a, $\Delta = \sim 10.1$ mV) compared with the drop-casting sensors (Fig. 6a, $\Delta = \sim 19.1$ mV), which well corresponded to the adhesion test results (Fig. 4a) that the electrosprayed S-ISM sensors possessed a strong membrane adhesion and negligible water layer formation. The concentration readings (mg/L) were converted from the potential readings (mV) recorded every 30 s

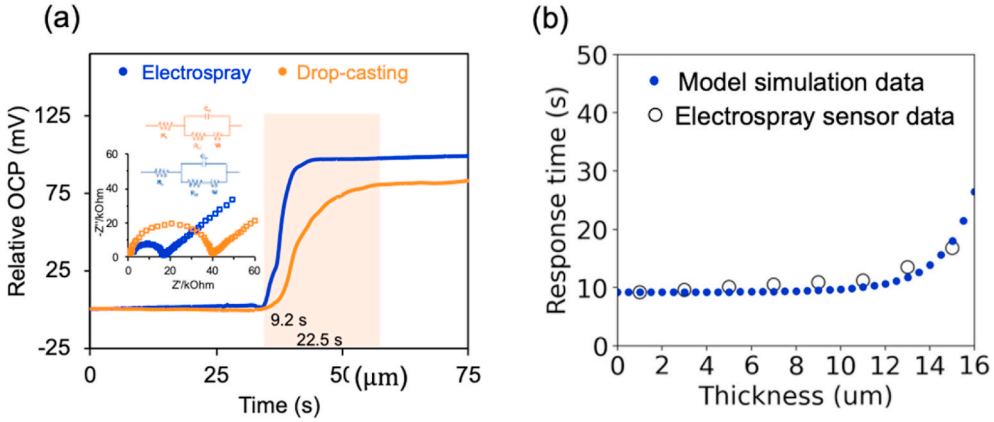

Fig. 5. (a). Variation of the response time of the electrosprayed sensors with the S-ISM membrane thickness. (b). The response time of the electrosprayed (membrane thickness: 1 μm) and drop-casting (membrane thickness: 25 μm) S-ISM sensors. (The insert diagram illustrates the impedance analysis of these two types of sensors).

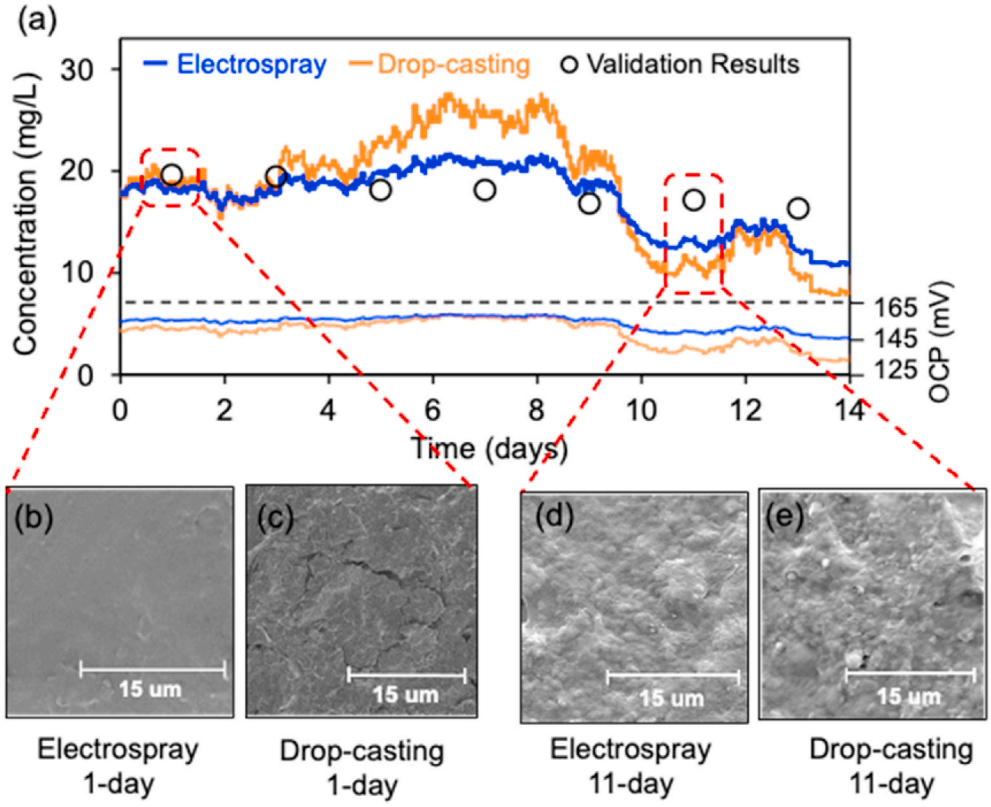

Fig. 6. (a) The potential readings (mV) and NH_4^+ concentration results (mg/L) of the electrosprayed and drop-casting S-ISM sensors in the continuous monitoring test in wastewater for 14 days. (b–e) the SEM images of the sensor surface throughout the test period.

through the calibration slopes (Fig. 6a), and verified against the standard ammonium dimethylphenol method (hollow dots in Fig. 6a). The discrepancy between the electrosprayed S-ISM NH_4^+ sensor results (blue line, Fig. 6a) and the validation results was less than 2.9 mg/L throughout the first 10 days, while drop-casting sensor exhibited a visibly larger discrepancy (>7.2 mg/L) in the same period, indicating a much more reliable dataset provided by the electrosprayed sensor (e.g., excellent sensitivity (55.28 mV/dec) and accuracy (R^2 = 0.9998), Fig. 3). Nevertheless, the accuracy of the electrosprayed sensor declined after 10 days, with the discrepancy higher than 4 mg/L in last two dots (day 11 and day 13). The SEM images showed high amounts of microbial cells attached onto the membrane surface (Fig. 6b-e). This surface fouling problem undoubtedly inhibited the permeability of NH_4^+ ions from bulk wastewater to the sensor surface, and thus impairing the sensor accuracy. In our previous study, 5% of the super-hydrophobic poly(tetrafluoroethylene) (PTFE) was incorporated into S-ISM polymer matrix to enhance the sensor anti-fouling capability [32]. However, PTFE could not be used for electrospray in this study, since the high viscosity of PTFE mixture blocked the emerging jet coming out the needle tip, resulting in the failure of forming of fine cocktail droplets with a diameter of nanometers (e.g., 200 nm). In fact, traditional liquid-state ISM sensors cannot last in the real wastewater for more than 24 h due to their friability and membrane fouling [49]. The commercial ammonium S-ISM sensors were unable to continuously monitor wastewater for ~30 min, suffered from severe reading drifting, and had to be taken out from wastewater every 30 min for cleaning by manually paper-wiping sensor surface. Although other modified ion selective sensors (e.g., microfluidic ammonium sensors [50], imprinted gold nanoparticle glycerol sensors [51] and naphthalimide-based copper sensors [52]) could last for 7 days in pure solution under static conditions, such test scenario was utterly different from the real-world wastewater test conducted in this study. In contrast, our electrosprayed S-ISM sensor without anti-fouling protection performed remarkably in wastewater with the error of less than 2.9 mg/L after continuously monitoring for 10 days, revealing a great potential for further enhancement.

3.5. *The future studies of conquering the long-term wastewater challenges*

We have demonstrated the fabrication of ultra-thin S-ISM membrane (thickness: 1 μm) using the electrospray technique, resulting in advanced characteristics (e.g., strong adhesion between S-ISM and electrode, fast response, and high sensitivity) of S-ISM sensors. Tests of continuous monitoring in wastewater for 14 days evidently displayed the improvement of the electrosprayed S-ISM sensors over the regular drop-casting S-ISM sensors. The experimental results well corresponded with the simulation data of the response model that established the correlation between the sensor response time and the ion diffusion in the S-ISM polymer matrix.

Although electrospray substantially enhanced the S-ISM characteristics and morphology, fabrication process is more time-consuming and costly than drop-casting due to high electricity input and motor energy and labor [19]. Additionally, electrospray technology could not augment the anti-fouling capability for S-ISM sensors (Fig. 1c), explicated by the deteriorated accuracy of the electrosprayed sensor after 10 days in wastewater (Fig. 6). Conventional anti-fouling protection membrane (e.g., polyvinylidene fluoride ultrafiltration membrane [53], PVDF (polyvinylidene fluoride) composite membrane [54]) typically results in a thick layer being formed on the sensor surface that ultimately impedes ion diffusion and impairs the sensor's response, stability and sensitivity. This study ushers a potential for using electrospray to deposit anti-fouling protection membrane onto the sensor surface to further enhance the sensors' long-term accuracy and durability in wastewater.

4. Conclusions

Electrospray printing technology, for the first time, was successfully deployed in the preparation of ultra-thin solid-state ion selective membrane (S-ISM) sensors. According to the cross-sectional SEM images, the thickness of electrosprayed S-ISM was reduced to as little as ~1 μm, which effectively enhanced the sensor characteristics including ionophore distribution, membrane morphology, sensor sensitivity, response time and accuracy. The response measurement showed the acceleration of sensor response from 22.5 s to 9.2 s, which was confirmed by the response model ($R^2 > 0.85$) elucidating that the fast ion diffusion in the electrosprayed S-ISM polymer matrix shortened the response time. As supported by the water layer test, the strong adhesion of electrosprayed S-ISM highly mitigated the water layer formation between the sensing membrane and the electrode, and thus alleviating the reading drifts (mV) and enhancing the sensor stability (0.66 mV/h). The electrosprayed S-ISM sensor performed remarkably in wastewater with an error of less than 2.9 mg/L after continuously monitoring for 10 days, exhibiting much enhanced performance then regular drop-casting S-ISM sensors. The success of electrosprayed S-ISM membrane in this study reveals a possibility of using electrospray to deposit an anti-fouling membrane layer onto the sensor surface in future studies to further ameliorate the long-term accuracy and stability of S-ISM sensors in water and wastewater monitoring.

Authorship contributions

Category 1.

Conception and design of study: Yingzheng Fan, Xin Qian, Jeffrey R. McCutcheon, Baikun Li. **Acquisition of data:** Yingzheng Fan, Xin Qian, Xingyu Wang, Thomas Funk, Brianna Herman.

Analysis and/or interpretation of data: Yingzheng Fan, Xin Qian, Jeffrey R. McCutcheon, Baikun Li.

Category 2.

Drafting the manuscript: Yingzheng Fan, Xin Qian, Xingyu Wang, Jeffrey R. McCutcheon, Baikun Li.

Revising the manuscript critically for important intellectual content: Yingzheng Fan, Xin Qian, Xingyu Wang, Jeffrey R. McCutcheon, Baikun Li.

Category 3.

Approval of the version of the manuscript to be published (the names of all authors must be listed):

Yingzheng Fan, Xin Qian, Xingyu Wang, Thomas Funk, Brianna Herman, Jeffrey R. McCutcheon, Baikun Li.

Human rights

This article does not contain any studies with human subjects performed by the any of the authors.

Animal studies

All institutional and national guidelines for the care and use of laboratory animals were followed.

Declaration of competing interest

Baikun Li declares that she has no conflict of interest. None of the coauthors has conflict of interest. The study was supported by National Science Foundation (NSF, USA), Connecticut SPARK Program and Infiltrator Co.

Acknowledgement

This study was supported by National Science Foundation (NSF) Environmental Engineering Program GOALI Project (Grant No.: 1706343), NSF Signal in the soil (SitS) Project (Grant No: 1935599), NSF CMMI (Grant No.: 2001544), NSF SCC project (Grant No.: ECCS-2018492), National Academy of Sciences (NAS) U.S.-Egypt S&T Joint Fund (2000009132) and Connecticut SPARK Program. Some experiments are supported by Infiltrator Water Technologies Co.

Appendix A. Supplementary data

Supplementary data to this article can be found online at https://doi.org/10.1016/j.memsci.2021.119997.

References

[1] Y. Huang, T. Wang, Z. Xu, E. Hughes, F. Qian, M. Lee, Y. Fan, Y. Lei, C. Brückner, B. Li, Real-time in situ monitoring of nitrogen dynamics in wastewater treatment processes using wireless, solid-state, and ion-selective membrane sensors, Environ. Sci. Technol. (2019) 53, https://doi.org/10.1021/acs.est.8b05928.

[2] Y. Fan, Z. Xu, Y. Huang, T. Wang, S. Zheng, A. DePasquale, C. Brüeckner, Y. Lei, B. Li, Long-term continuous and real-time in situ monitoring of Pb(II) toxic contaminants in wastewater using solid-state ion selective membrane (S-ISM) Pb and pH auto-correction assembly, J. Hazard Mater. 400 (2020) 109891, https://doi.org/10.1016/j.jhazmat.2020.123299.

[3] C. Bieg, K. Fuchsberger, M. Stelzle, Introduction to polymer-based solid-contact ion-selective electrodes—basic concepts, practical considerations, and current research topics, Anal. Bioanal. Chem. 409 (2017) 45–61, https://doi.org/10.1007/s00216-016-9945-6.

[4] G.A. Crespo, Recent Advances in Ion-selective membrane electrodes for in situ environmental water analysis, Electrochim. Acta (2017), https://doi.org/10.1016/j.electacta.2017.05.159.

[5] M. Novell, M. Parrilla, G.A. Crespo, F.X. Rius, F.J. Andrade, Paper-based ion-selective potentiometric sensors, Anal. Chem. (2012), https://doi.org/10.1021/ac202979j.

[6] K. Liu, X. Jiang, Y. Song, R. Liang, Robust fabrication of nanomaterial-based all-solid-state ion-selective electrodes, RSC Adv. (2019), https://doi.org/10.1039/c9ra02770j.

[7] Y. Fan, F. Qian, Y. Huang, I. Sifat, C. Zhang, A. Depasquale, L. Wang, B. Li, Miniature microbial fuel cells integrated with triggered power management systems to power wastewater sensors in an uninterrupted mode, Appl. Energy 302 (2021) 117556, https://doi.org/10.1016/j.apenergy.2021.117556.

[8] J. Wang, R. Liang, W. Qin, Thin polymeric membrane ion-selective electrodes for trace-level potentiometric detection, Anal. Chim. Acta 1139 (2020) 1–7, https://doi.org/10.1016/j.aca.2020.09.024.

[9] S. Papp, M. Bojtár, R.E. Gyurcsányi, T. Lindfors, Potential reproducibility of potassium-selective electrodes having perfluorinated alkanoate side chain functionalized poly(3,4-ethylenedioxytiophene) as a hydrophobic solid contact, Anal. Chem. 91 (2019) 9111–9118, https://doi.org/10.1021/acs.analchem.9b01587.

[10] T. Han, U. Mattinen, J. Bobacka, Improving the sensitivity of solid-contact ion-selective electrodes by using coulometric signal transduction, ACS Sens. 4 (2019) 900–906, https://doi.org/10.1021/acssensors.8b01649.

[11] M.P.S. Mousavi, A. Ainla, E.K.W. Tan, M. Abd El-Rahman, Y. Yoshida, L. Yuan, H. H. Sigurslid, N. Arkan, M.C. Yip, C.K. Abrahamsson, S. Homer-Vanniasinkam, G. M. Whitesides, Ion sensing with thread-based potentiometric electrodes, Lab Chip 18 (2018) 2279–2290, https://doi.org/10.1039/c8lc00352a.

[12] M.R. Chowdhury, J. Steffes, B.D. Huey, J.R. McCutcheon, Supplementary: 3D printed polyamide membranes for desalination, Science 361 (2018) 682–686, https://doi.org/10.1126/science.aar2122.

[13] M.R. Chowdhury, J. Steffes, B.D. Huey, J.R. Mccutcheon, 3D printed polyamide membranes for Desalination, Science 686 (2018) 682–686.

[14] P. Kebarle, A brief overview of the present status of the mechanisms involved in electrospray mass spectrometry, J. Mass Spectrom. (2000), https://doi.org/10.1002/1096-9888(200007)35:7<804::AID-JMS22>3.0.CO;2-Q.

[15] N. Ju, Y. Yamagata, T. Higuchi, Thin-film fabrication method for organic light-emitting diodes using electrospray deposition, Adv. Mater. (2009), https://doi.org/10.1002/adma.200900444.

[16] S. Kavadiya, P. Biswas, Electrospray deposition of biomolecules: applications, challenges, and recommendations, J. Aerosol Sci. (2018), https://doi.org/10.1016/j.jaerosci.2018.04.009.

[17] X. Fan, Y. Xu, C. Ma, W. He, In-situ growth of Co3O4 nanoparticles based on electrospray for an acetone gas sensor, J. Alloys Compd. 854 (2021) 157234, https://doi.org/10.1016/j.jallcom.2020.157234.

[18] A.P. Taylor, L.F. Velásquez-García, Electrospray-printed nanostructured graphene oxide gas sensors, Nanotechnology 26 (2015) 505301, https://doi.org/10.1088/0957-4484/26/50/505301.

[19] X. Qian, T. Ravindran, S.J. Lounder, A. Asatekin, J.R. McCutcheon, Printing zwitterionic self-assembled thin film composite membranes: tuning thickness leads to remarkable permeability for nanofiltration, J. Membr. Sci. 635 (2021), https://doi.org/10.1016/j.memsci.2021.119428, 119428.

[20] J. Friedrich, K. Altmann, S. Wettmarshausen, G. Hidde, Coating of Carbon Fibers with Adhesion-Promoting Thin Polymer Layers Using Plasma Polymerization or Electrospray Ionization Technique—A Comparison, Plasma Processes and Polymers, 2017, https://doi.org/10.1002/ppap.201600074.

[21] E. Bakker, P. Bühlmann, E. Pretsch, Carrier-based ion-selective electrodes and bulk optodes. 1. General characteristics, Chem. Rev. 97 (1997) 3083–3132, https://doi.org/10.1021/cr940394a.
[22] P. Bühlmann, E. Pretsch, E. Bakker, Carrier-based ion-selective electrodes and bulk optodes. 2. Ionophores for potentiometric and optical sensors, Chem. Rev. 98 (1998) 1593–1687, https://doi.org/10.1021/cr970113+.
[23] M.R. Chowdhury, J.R. McCutcheon, Elucidating the impact of temperature gradients across membranes during forward osmosis: coupling heat and mass transfer models for better prediction of real osmotic systems, J. Membr. Sci. 553 (2018) 189–199, https://doi.org/10.1016/j.memsci.2018.01.004.
[24] Y. Shao, Y. Ying, J. Ping, Recent advances in solid-contact ion-selective electrodes: functional materials, transduction mechanisms, and development trends, Chem. Soc. Rev. 49 (2020) 4405–4465, https://doi.org/10.1039/c9cs00587k.
[25] Y. Fan, Y. Huang, W. Linthicum, F. Liu, A.O. Beringhs, Y. Dang, Z. Xu, S.-Y. Chang, J. Ling, B.D. Huey, Toward long-term accurate and continuous monitoring of nitrate in wastewater using poly (tetrafluoroethylene)(PTFE)–Solid-State ion-selective electrodes (S-ISEs), ACS Sens. 5 (2020) 3182–3193.
[26] V.V. Egorov, A.D. Novakovskii, E.A. Zdrachek, Modeling of the effect of diffusion processes on the response of ion-selective electrodes by the finite difference technique: comparison of theory with experiment and critical evaluation, J. Anal. Chem. 72 (2017) 793–802, https://doi.org/10.1134/S1061934817070048.
[27] A.M. Gañán-Calvo, The surface charge in electrospraying: its nature and its universal scaling laws, J. Aerosol Sci. (1999), https://doi.org/10.1016/S0021-8502(98)00780-0.
[28] E. Bakker, P. Bühlmann, E. Pretsch, Carrier-based ion-selective electrodes and bulk optodes. 1. General characteristics, Chem. Rev. (1997), https://doi.org/10.1021/cr940394a.
[29] G.C. Ochoa, J.C. Aguilar-Cordero, Membrane composition effects on the analytical behavior of solid contact potentiometric pb2+ selective electrodes based on diazadibenzo-18-crown-6 ionophores, Electroanalysis (2011), https://doi.org/10.1002/elan.201100073.
[30] M. Guzinski, J.M. Jarvis, F. Perez, B.D. Pendley, E. Lindner, R. De Marco, G. A. Crespo, R.G. Acres, R. Walker, J. Bishop, PEDOT(PSS) as solid contact for ion-selective electrodes: the influence of the PEDOT(PSS) film thickness on the equilibration times, Anal. Chem. 89 (2017) 3508–3516, https://doi.org/10.1021/acs.analchem.6b04625.
[31] T.Y. Chiang, L.M. Fu, C.H. Tsai, C.H. Lin, Ion-selective membrane formed in a microfluidic chip utilizing surface tension force for high sensitive ammonia ion sensing, in: Proceedings of the 16th International Conference on Miniaturized Systems for Chemistry and Life Sciences, MicroTAS 2012, 2012.
[32] Y. Fan, Y. Huang, W. Linthicum, F. Liu, A.O. Beringhs, Y. Dang, Z. Xu, S. Chang, J. Ling, B.D. Huey, S.L. Suib, A.W. Ma, P. Gao, X. Lu, Y. Lei, M.T. Shaw, B. Li, Towards long-term accurate and continuous monitoring of nitrate in wastewater using PTFE (polytetrafluoroethylene)- solid-state ion-selective electrodes (S-ISEs), ACS Sens. (2020), https://doi.org/10.1021/acssensors.0c01422.
[33] C. Zuliani, D. Diamond, Opportunities and challenges of using ion-selective electrodes in environmental monitoring and wearable sensors, Electrochim. Acta (2012), https://doi.org/10.1016/j.electacta.2012.04.147.
[34] J. Hu, A. Stein, P. Bühlmann, Rational design of all-solid-state ion-selective electrodes and reference electrodes, Trac. Trends Anal. Chem. 76 (2016) 102–114, https://doi.org/10.1016/j.trac.2015.11.004.
[35] L. Ying, G. Ai-jun, Z. Jing, Study of treating high ammonia-N domestic wastewater with CASS process, Procedia Environmental Sciences 11 (2011) 858–863, https://doi.org/10.1016/j.proenv.2011.12.131.
[36] Y. Kan, C. Han, Y. Ye, X. Zhang, Y. Huang, L. Xing, Y. Zhou, H. Qin, An all-solid-state ammonium ion-selective electrode based on polyaniline as transducer and poly (o-phenylenediamine) as sensitive membrane, International Journal of Electrochemical Science (2016), https://doi.org/10.20964/2016.12.03.
[37] S.S.M. Hassan, A.G. Eldin, A.E.G.E. Amr, M.A. Al-Omar, A.H. Kamel, N.M. Khalifa, Improved solid-contact nitrate ion selective electrodes based on multi-walled carbon nanotubes (MWCNTs) as an ion-to-electron transducer, Sensors (2019), https://doi.org/10.3390/s19183891.
[38] M.K.A. El-Rahman, M.R. Rezk, A.M. Mahmoud, M.R. Elghobashy, Design of a stable solid-contact ion-selective electrode based on polyaniline nanoparticles as ion-to-electron transducer for application in process analytical technology as a real-time analyzer, Sensor. Actuator. B Chem. (2015), https://doi.org/10.1016/j.snb.2014.11.009.
[39] J.P. Veder, R. De Marco, G. Clarke, R. Chester, A. Nelson, K. Prince, E. Pretsch, E. Bakker, Elimination of undesirable water layers in solid-contact polymeric ion-selective electrodes, Anal. Chem. 80 (2008) 6731–6740, https://doi.org/10.1021/ac800823f.
[40] F. Sundfors, L. Höfler, R.E. Gyurcsányi, T. Lindfors, Influence of poly(3-octylthiophene) on the water transport through methacrylic-acrylic based polymer membranes, Electroanalysis 23 (2011) 1769–1772, https://doi.org/10.1002/elan.201100076.
[41] J. Ping, Y. Wang, J. Wu, Y. Ying, Development of an all-solid-state potassium ion-selective electrode using graphene as the solid-contact transducer, Electrochem. Commun. 13 (2011) 1529–1532, https://doi.org/10.1016/j.elecom.2011.10.018.
[42] L. Zhao, Y. Jiang, J. Hao, H. Wei, W. Zheng, L. Mao, Graphdiyne oxide enhances the stability of solid contact-based ionselective electrodes for excellent in vivo analysis, Sci. China Chem. (2019), https://doi.org/10.1007/s11426-019-9516-5.
[43] B. Paczosa-Bator, Ion-selective electrodes with superhydrophobic polymer/carbon nanocomposites as solid contact, Carbon (2015), https://doi.org/10.1016/j.carbon.2015.09.006.
[44] N. Kaur, J. Kaur, R. Badru, S. Kaushal, P.P. Singh, BGO/AlFu MOF core shell nanocomposite based bromide ion-selective electrode, Journal of Environmental Chemical Engineering (2020), https://doi.org/10.1016/j.jece.2020.104375.
[45] F. Criscuolo, I. Taurino, F. Stradolini, S. Carrara, G. De Micheli, Highly-stable Li+ ion-selective electrodes based on noble metal nanostructured layers as solid-contacts, Anal. Chim. Acta (2018), https://doi.org/10.1016/j.aca.2018.04.062.
[46] H. Karami, M.F. Mousavi, Dodecyl benzene sulfonate anion-selective electrode based on polyaniline-coated electrode, Talanta (2004), https://doi.org/10.1016/j.talanta.2003.12.025.
[47] E. Bakker, Membrane response model for ion-selective electrodes operated by controlled-potential thin-layer coulometry, Anal. Chem. 83 (2011) 486–493, https://doi.org/10.1021/ac102016y.
[48] V.V. Egorov, A.D. Novakovskii, E.A. Zdrachek, An interface equilibria-triggered time-dependent diffusion model of the boundary potential and its application for the numerical simulation of the ion-selective electrode response in real systems, Anal. Chem. 90 (2018) 1309–1316, https://doi.org/10.1021/acs.analchem.7b04134.
[49] D.P. Manica, Y. Mitsumori, A.G. Ewing, Characterization of electrode fouling and surface regeneration for a platinum electrode on an electrophoresis microchip, Anal. Chem. (2003), https://doi.org/10.1021/ac034235f.
[50] J. Gallardo-Gonzalez, A. Baraket, S. Boudjaoui, T. Metzner, F. Hauser, T. Rößler, S. Krause, N. Zine, A. Streklas, A. Alcácer, J. Bausells, A. Errachid, A fully integrated passive microfluidic Lab-on-a-Chip for real-time electrochemical detection of ammonium: sewage applications, Sci. Total Environ. (2019), https://doi.org/10.1016/j.scitotenv.2018.11.002.
[51] S. Motia, B. Bouchikhi, E. Llobet, N. El Bari, Synthesis and characterization of a highly sensitive and selective electrochemical sensor based on molecularly imprinted polymer with gold nanoparticles modified screen-printed electrode for glycerol determination in wastewater, Talanta (2020), https://doi.org/10.1016/j.talanta.2020.120953.
[52] I.J. Chang, M.G. Choi, Y.A. Jeong, S.H. Lee, S.K. Chang, Colorimetric determination of Cu2+in simulated wastewater using naphthalimide-based Schiff base, Tetrahedron Lett. (2017), https://doi.org/10.1016/j.tetlet.2016.12.066.
[53] J. Zhang, Z. Xu, M. Shan, B. Zhou, Y. Li, B. Li, J. Niu, X. Qian, Synergetic effects of oxidized carbon nanotubes and graphene oxide on fouling control and anti-fouling mechanism of polyvinylidene fluoride ultrafiltration membranes, J. Membr. Sci. 448 (2013) 81–92, https://doi.org/10.1016/j.memsci.2013.07.064.
[54] X. Lu, Y. Peng, L. Ge, R. Lin, Z. Zhu, S. Liu, Amphiphobic PVDF composite membranes for anti-fouling direct contact membrane distillation, J. Membr. Sci. 505 (2016) 61–69, https://doi.org/10.1016/j.memsci.2015.12.042.